Int. J. Electrochem. Sci., 8 (**2013**) 6664 - 6677

International Journal of
ELECTROCHEMICAL
SCIENCE
www.electrochemsci.org

Polarization Behavior of Electroless Ni-P Plating on Magnesium Alloys

Zhihui Xie[1], Gang Yu[1,], Bonian Hu[2,*], Xueyuan Zhang[1,*], Laibing Li[2], Wenge Wang[2], Dechun Zhang[2]*

[1] State Key Laboratory of Chemo/Biosensing and Chemometrics, College of Chemistry and Chemical Engineering, Hunan University, Changsha 410082, P. R. China
[2] Department of Materials and Chemical Engineering, Hunan Institute of Technology, Hunan, Hengyang 421002, P. R. China
[*]E-mail: yuganghnu@163.com; hbonian@yahoo.com.cn; uwoxyzhang@gmail.com

Received: 6 March 2013 / *Accepted:* 2 April 2013 / *Published:* 1 May 2013

In order for obtaining more kinetics information of the electroless Ni-P (EN) plating processes, the electrochemical behavior of EN coating on Mg alloys in different baths was investigated with polarization curves. The deposition rates of EN alloys were compared and discussed by gravimetrical measurement and electrochemical measurement. The influences of concentration of nickel ions, hypophosphite and hydrogen ion on the polarization curves and EN deposition in a complete bath were also studied and discussed. From these variations in the deposition potential and current density, a kinetic expression employing the Butler-Volmer equation and mixed potential theory was set up and was in good agreement with the experimental findings. It was confirmed that the electroless nickel deposition processes in the present researches was under a mixed control. The apparent activation energy of the alloy deposition was also determined to be 42.89 $kJ\cdot mol^{-1}$ by electrochemical methods. Electrochemical polarization measurement in the complete bath could be effective to monitor EN deposition rate.

Keywords: Electroless Ni-P plating; Deposition rate; Polarization curves; Monitoring; Mixed potential theory

1. INTRODUCTION

Magnesium alloys are extensively used in aerospace, defense, auto parts, e-communication, optical instruments and portable personal computers, etc, because of their excellent physical and mechanical properties 1. However, an obstacle to their further applications lies in their high chemical and electrochemical reactivity which makes them prone to oxidation and corrosion in humid atmosphere, fresh water, seawater, most of organic acids and inorganic acids 2. Electroless nickel-phosphorus (EN) plating is widely used to improve the performance due to uniform coverage and high

corrosion resistance of obtained deposits on Mg alloys 3. In spite of this, most studies on EN deposition were focused on the pretreatment [4, 5] or post-treatment 6 of the substrates, structure 7, magnetism 8, mechanical and anticorrosion behavior of deposits 9, the effects of additives on the bath stability 10. Limited results were reported relating to the influence of surface microstructure of the substrate on the initial deposition mechanism [11-13] and deposition dynamics 14 or growth kinetics of deposits 15. However, there are still some arguments to understand the mechanistic aspects of these processes.

Five classical mechanisms have been proposed to explain electroless deposition of metal and alloys [3, 16] as follows. (1) Atomic hydrogen mechanism. (2) Hydride ion mechanism. (3) Metal hydroxide mechanism. (4) Electrochemical mechanism. (5) Uniform mechanism 17. In all of the above mechanisms, electrochemical mechanism not only provided a simple and obvious reaction processes, but also invoked a strictly electrochemical approach which may predict the deposition rate with mixed potential theory according to the anodic and cathodic polarization curves 3. According to electrochemical mechanism, electroless deposition was resulted from mixed anodic and cathodic reactions. In the case of EN deposition using hypophosphite as reducing agent, anodic partial process was the oxidation of reducer with water, and the electrons generated in the anodic reaction were utilized in the coupled cathodic processes for deposition of Ni and P. Meanwhile, the evolution of hydrogen gas was account for a result of the secondary reaction of hydrogen ions 16. The partial polarization measurement based on the electrochemical mechanism was thought a very reliable method of estimating the deposition rate in the case of electroless Cu [18-21], Ni-P 22, Au [18, 23], Co-P [24-25], and Ag (W) 26. However, extrapolation of the anodic and cathodic curves to obtain a deposition current density also gave deviation results in comparison with weight gain measurements in many varieties of electroless metals, such as Cu [27-30], Co [31-32], Ni-P 33. These investigations show that electroless plating of different metal alloys or deposition on different substrates may not be involved in the same deposition dynamical processes.

A considerable controversy still exists on whether the rate of electroless plating could be determined by the deposition current density from a complete plating bath or from the intersection of the partial anodic and cathodic polarization curves. Moreover, to the best of our knowledge, no results have been reported on electrochemical behavior of EN plating on magnesium alloys until now. Thus, according to the literature review, more work is required to understand fundamental issues related to the kinetic mechanisms and the influence of process parameters on electrochemical behavior of the EN. The deposition potential and deposition current density of the EN plating was studied by changing the concentration of metal salt, reducer, bath acidity and temperature. The deposition rate theoretically derived from the current-potential (*I-E*) curves in a complete bath was compared with that with gravimetrical measurement in order for an investigation on the mechanism of Ni-P deposition.

2. EXPERIMENTAL

The samples used for the investigation were prepared (in the form of plates $30 \times 20 \times 2$ mm^3) from a plain die cast of magnesium alloy (AZ91D) from Boao Mg Co. Ltd., China. The magnesium

substrate was orderly polished with #600, #1500 silicon carbide waterproof abrasive paper, then decreased in acetone and an alkaline solution, and finally pickled in an acidic solution in sequence prior to deposition in a 250 cm^3 plastic beaker. The chemical compositions of the alloy and more detailed pretreatment processes could be found in our precious work 34. The complete bath components and plating conditions are presented in Table 1.

Table 1. The complete bath composition of EN plating

Composition	Quantity	Condition
$NiSO_4·6H_2O$	15~35 $g·dm^{-3}$	pH: 4~6
$NaH_2PO_2·H_2O$	15~35 $g·dm^{-3}$	351~363 K
$C_6H_8O_7·H_2O$	5 $g·dm^{-3}$	60 min
HF (40%)	12 $cm^3·dm^{-3}$	
NH_4HF_2	10 $g·dm^{-3}$	
$CS(NH_2)_2$	1 $mg·dm^{-3}$	
$NH_3·H_2O$ (25%)	App. 30 $cm^3·dm^{-3}$	pH adjustor

The average deposition rate (v_w: $\mu m·h^{-1}$) determined by the gravimetrical method during the deposition process could be calculated according to the following formula:

$$v_w = \frac{10(w_t - w_0)}{A_s \rho t} \qquad (1)$$

where w_0 (mg) and w_t (mg) are the weight of the samples before and after electroless plating respectively, A_s (cm^2) is the surface area of specimen, ρ ($g·cm^{-3}$) is the density of the deposit (assuming a bulk density of 7.8 $g·cm^{-3}$) and t (h) is the plating duration.

The instantaneous deposition rate (v_i, $mg·cm^{-2}·h^{-1}$) was calculated as follows:

$$v_i = \frac{i_{dep} M}{zF} = 1.08 i_{dep} \qquad (2)$$

where F is the Faraday constant($C·mol^{-1}$), M the molar mass of Ni-P deposits (supposing M= 58 $g·mol^{-1}$), z the number of electrons obtained by nickel ions, i_{dep} is the deposition current density ($mA·cm^{-2}$) from the polarization measurement.

The electrochemical measurement was carried out in a three-electrode cell system with the electrochemical analyzer Reference 600 (Gamry, America). A nickel plate was embedded in an epoxy resin, leaving a 1×1 cm^2 effective working area, as the working electrode. The auxiliary electrode was a platinum foil with a size of 20 mm × 20 mm. The potential of the working electrode was measured against a saturated calomel electrode (SCE) via a Luggin capillary and a salt bridge. Polarization measurements were carried out in various baths with a scan rate of 5 $mV·s^{-1}$. The pH of the solution

was measured by electronic pH-meter (Mettler Toledo, FE20 - FiveEasy). All the experimental temperature was controlled by a digitally controlled thermostatic water bath.

3. RESULTS AND DISCUSSION

3.1 Open-circuit potential and polarization curves in three solutions

The change of open circuit potential (OCP) of nickel electrode in three different solutions at 358K is shown in Fig. 1 The OCP shift sharply towards more negative in the first few seconds, and then it reached a constant after 400 s of immersion in the three different solutions. The steady OCP of Ni in a complete plating bath (Curve a in Fig. 1, −0.6523 V) was lower than that of a solution either without reducing agent (Curve b in Fig. 1, −0.4285 V) or metal salt (Curve c in Fig. 1, −0.4702 V). This difference of steady potential in three plating bath indicated that the sum of partial contributions could not represent the experimental result obtained in a complete solution. This potential difference was confirmed by the polarization curves in various solutions, as shown in Fig. 2.

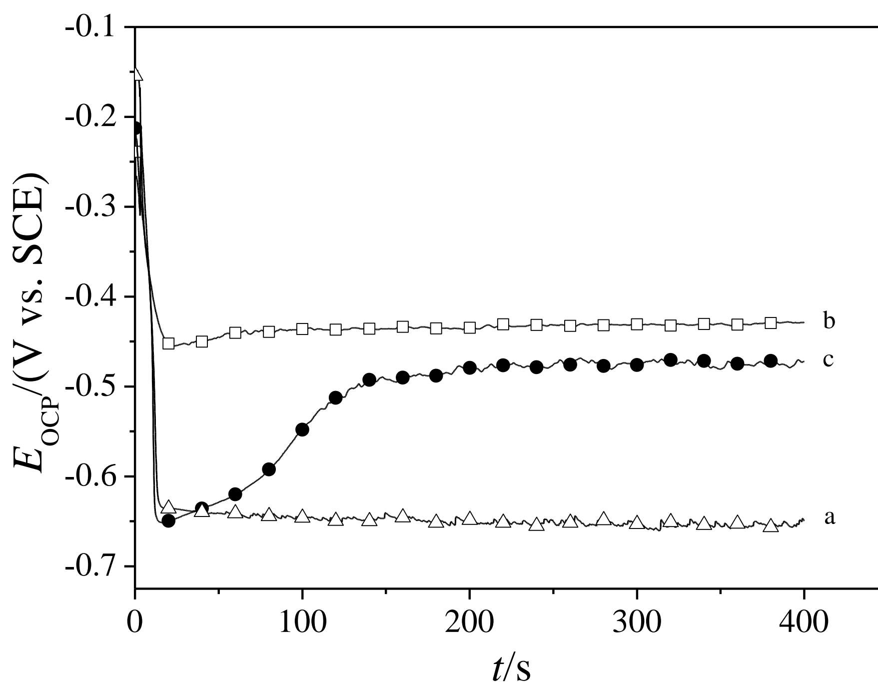

Figure 1. Curves of OCP-time in solutions: (a) complete plating bath, (b) in the absence of reducing agent and (c) in the absence of metallic salt（$NiSO_4 \cdot 6H_2O$ 20 g·dm^{-3} $NaH_2PO_2 \cdot H_2O$ 20 g·dm^{-3}）

According to the mixed potential theory 16, EN deposition could be predicted from the anodic and cathodic processes occurred on Mg alloy. As a ruler, mixed potential theory is assumed that EN

plating can be considered as the superposition of anodic partial (reductant oxidation) and cathodic (metal reduction) partial reaction at the mixed potential, E_{mix} as shown in Fig. 2. In the case of electrochemical oxidation of hypophosphite as a main anodic reaction in the acid plating bath, and the cathodic reaction was mainly caused by the reduction of Ni^{2+}, the contribution from P deposit and hydrogen evolution was neglected.

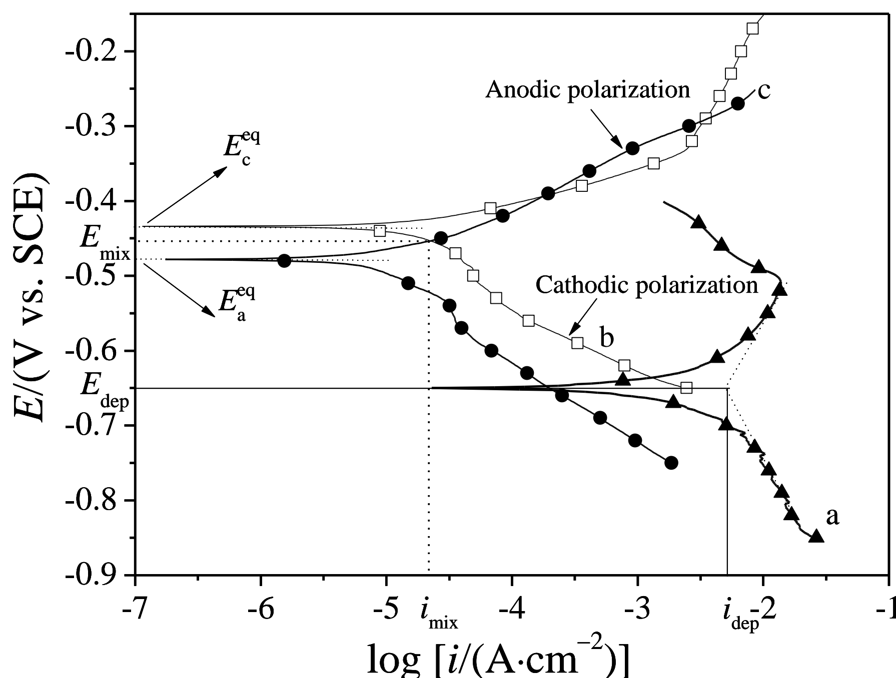

Figure 2. Polarization curves in different baths: (a) complete plating bath, (b) in the absence of reducing agent and (c) in the absence of metallic salt（$NiSO_4 \cdot 6H_2O$ 20 g·dm^{-3} $NaH_2PO_2 \cdot H_2O$ 20 g·dm^{-3}）

The anodic and cathodic reactions proceed through the following reactions.

Cathodic: $NiL_m^{2+} + 2e^- \rightarrow Ni + mL$ (3)

$$E_c^{eq} = E^{\ominus}_{NiL_m^{2+}/Ni} + \frac{1.152RT}{F}\beta_m + \frac{1.152RT}{F}\log[Ni^{2+}] \quad (4)$$

Anodic: $H_2PO_2^- + H_2O \rightarrow H_2PO_3^- + 2H^+ + 2e^-$ (5)

$$E_a^{eq} = E^{\ominus}_{H_2PO_3^-/H_2PO_2^-} + \frac{1.152RT}{F}\log\frac{[H_2PO_3^-][H^+]^2}{[H_2PO_2^-]} \quad (6)$$

where R is the gas constant, T is the temperature, F is Faraday constant, β_m is stability constant of the complex, and $E^{\ominus}$ is the corresponding standard redox potential of reaction. Accordingly, the

rates of the deposition could be estimated by the corresponding current density at the superposition point (i_{mix} in Fig. 2; E^{eq} is the equilibrium potential of corresponding partial reaction). The electroless deposition current density obtained in a complete bath (i_{dep} in Fig. 2) in the same conditions is more than one hundred times higher than the predicted current density by mixed potential theory (i_{mix}), while the deposition potential (E_{dep}) from the former in a complete bath is lower than that from the latter (E_{mix}) (in incomplete bath). It is shown in Fig. 2 that there is an abnormal current depression in the anodic branch of the polarization curves in a complete bath, which is not observed in the absence of nickel ions. Further, the anodic and cathodic processes appear to interdependent 32. One of the most important reasons to explain this phenomenon can be ascribed to the reduction of metal ions involves many more electrons than those provided by the anodic partial reactions 33. Another possible reason is the freshly nucleated nickel grains have a favorable catalytic effect on the oxidation of hypophosphite 35. Thus, a complete plating bath, not an electrolyte in absence of either reducer or nickel ion was chosen as the electrochemical mechanism investigation system in the present work.

3.2 Effect of ion concentrations and plating temperature on the bath electrochemical behavior

There are several variables which influence the deposition processes during the elecroless nickel plating. The main factors to control the deposition rate, i.e. bath acidity, temperature, the concentration of metal salt and hypophosphite, will be discussed in our present work. Fig. 3 presents the dependence of the deposition potential (E_{dep}), current density (i_{dep}) and deposition rate on the concentration of nickel salt. Curve A in Fig. 3 shows that the deposition potential increases linearly with increasing concentration of nickel sulfate, and it could be explained by the Nernst′s equations.

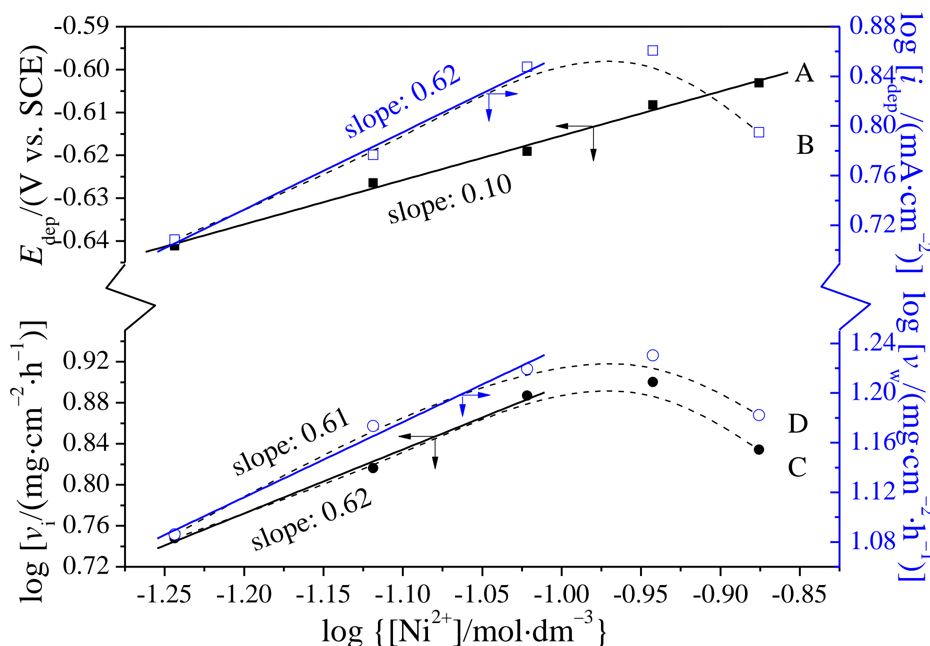

Figure 3. Dependence of the deposition potential (A), current density (B) and deposition rate (C: derived from the current density of curve B by Faraday's law; D: obtained by gravimetrical method) on the $NiSO_4$ concentration for EN deposition

It can be seen from Eq. (4) that a proportional linear relationship is established between the cathodic equilibrium potential and the logarithm of the concentration of nickel salt. Therefore, assuming the anodic equilibrium potential is held at a relatively constant, the deposition potential of the electroless deposition processes would be shift to the positive direction when the concentration of nickel sulfate was increased. The deposition current density increased firstly and then decreased with the concentration of nickel sulfate in the range of 15~35 $g{\cdot}dm^{-3}$ as shown curve B in Fig. 3. Similar observations have also been made by other researchers [36-37], the explanation for this phenomenon might be related to the total number of moles of adsorbed ions species on the electrode surface 14.

As shown in curve C and D in Fig. 3, the deposition rates by gravimetrical measurement and electrochemical measurement show a similar trend, i.e., the concentration of nickel sulfate to reach a maximum deposition rate, is almost identical. Owing to the negligence of the evolution of hydrogen gas in the cathodic reactions, the instantaneous deposition rate calculated from electrochemical method is supposed to be higher than the average deposition rate determined from gravimetrical method. However, an opposite result was obtained in the present work. The possible reasons may be explained as follows. (1) the current densities obtained from the experimental polarization curve are always lower than the theoretical value 38. The experimental curves are apparent polarization curves, which indicate the relationship between the applied current density (which can be detected by an Ampere-meter) and the electrode potential, whereas, the theoretical polarization curves depict the relationship between the net current density and electrode potential of the anodic partial reaction and cathodic partial reaction proceeds simultaneously at one electrode surface.

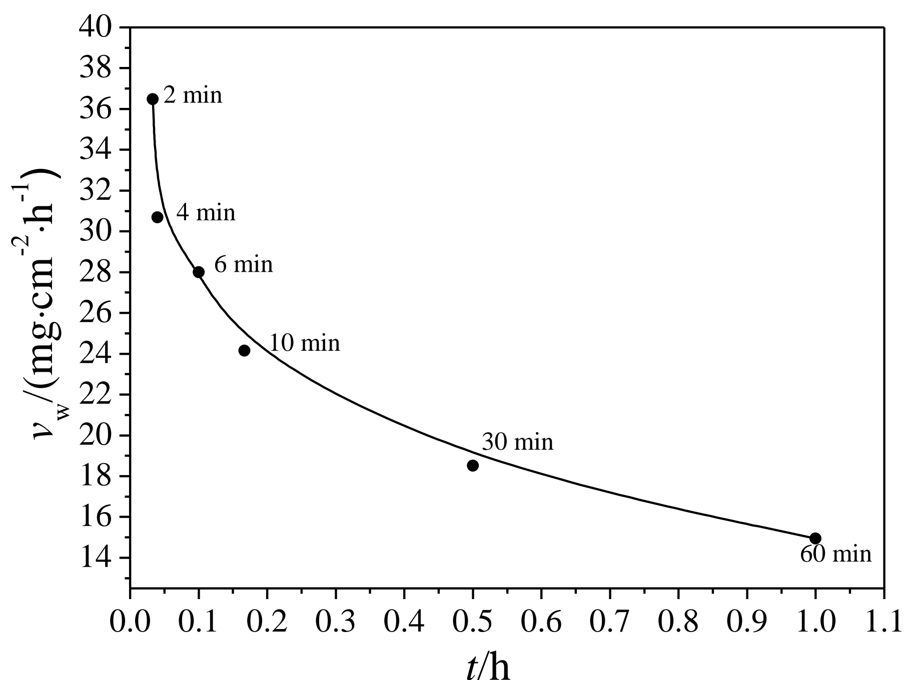

Figure 4. Deposition rate calculated by gravimetrical measurement on different deposition times

Therefore, the current densities determined by the electrochemical polarization are always lower than the theoretical values, exhibiting a lower instantaneous deposition rate here, and the

difference is more pronounced when the electrode was applied at a low overpotential; (2) the deposition rate determined through gravimetrical measurement describes a gradually decreased trend with immersion as shown in Fig. 4. After a drastically drop in the initial deposition time, the deposition rate declines slightly and reaches a value less than half of the initial rate at 60 min. This variation in the deposition rate may result from the different types of deposition reaction at different immersion time. A large number of active sites on the surface of magnesium alloys were formed after pretreatment processes. This lead to a replacement deposition occurred with autocatalytic deposition at the initial stage, while only autocatalytic deposition was observed after the substrate was totally covered by the coating 14. In addition, some diffusion control or electrode coverage with intermediate species involved in the hydrogen evolution process decrease the deposition rate as the deposition proceeds 39. Of course, another reason caused the changing of the deposition rate is the decreased concentration of nickel ions and reducer. Therefore, the average deposition rates determined from gravimetrical measurement are slightly higher than the instantaneous deposition rates calculated from electrochemical measurement.

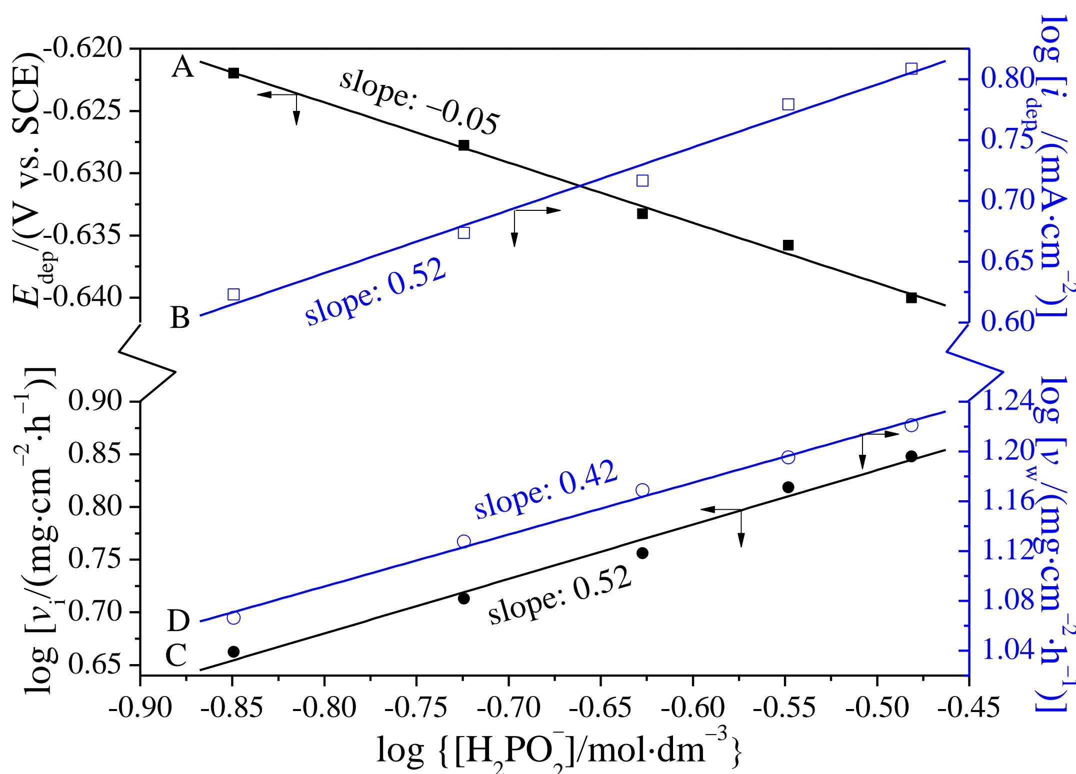

Figure 5. Dependence of the deposition potential (A), current density (B) and deposition rate (C: derived from the current density of curve B by Faraday's law; D: obtained by gravimetrical method) on the $NaH_2PO_2{\cdot}H_2O$ concentration for EN deposition

Variations of deposition potential, current density and deposition rate with the concentration of reducing agent are shown in Fig. 5, where it is seen that a higher concentration of reducer results in a decrease in deposition potential and an increase in deposition current density. According to Eq. (6), a higher concentration of hypophosphite decreases the anodic equilibrium potential, thereby brings the

deposition potential to a more noble value if the cathodic equilibrium potential keeps a constant. This effect of reducer on the potential is less remarkable comparing to the effect of metal salt on the potential. The influence of hypophosphite concentration on the deposition rate from two different measurements is shown in curve C and D in Fig. 5. The deposition rate increases with hypophosphite concentration, which has been demonstrated by other authors [21, 25]. This enhanced effect with increasing hypophosphite concentration may be attributed to a deprotonation reaction which is favorable for the nickel deposition 14. The effects of hypophosphite concentration on the deposition potential and deposition rate also demonstrate that the deposition potential determines the tendency of deposition reactions whereas the deposition current density determines the rate of the process.

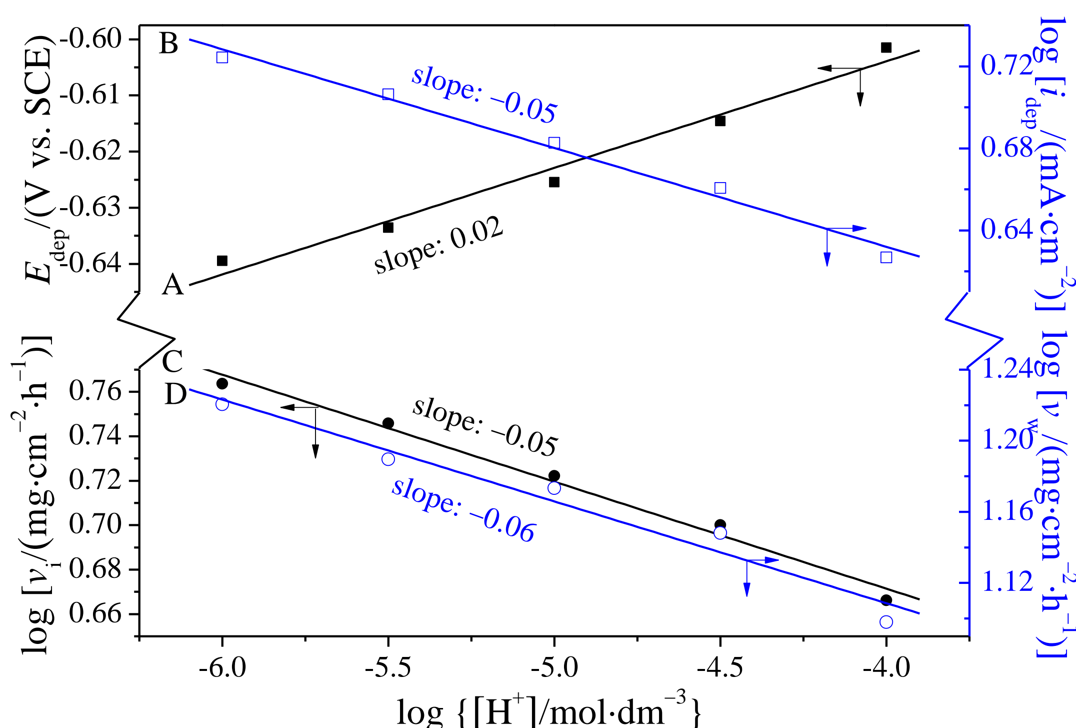

Figure 6. Dependence of the deposition potential (A), current density (B) and deposition rate (C: derived from the current density of curve B by Faraday's law; D: obtained by gravimetrical method) on the H^+ concentration for EN deposition

As shown in Fig. 6, the concentration of hydrogen ion in the plating bath plays an important role in both deposition potential and current density. Curve C and D in Fig. 6 illustrate the deposition rate determined from two different methods decreased with increasing the concentration of hydrogen ions. Those curves indicated that the deposition reactions were depressed both in aspects of dynamics and thermodynamics when hydrogen ion in the bath increased. It is well known that an increase in the concentration of hydrogen ion results in a decrease in the concentration of the free nickel ions, which leads to a decrease of the equilibrium potential of cathodic partial reaction according to Eq. (4). Therefore, the positive shift of the deposition potential with increasing hydrogen ion concentration may not be only ascribed to the decrease of the anodic equilibrium potential from Eq. (6), but also the variation of the cathodic equilibrium potential. According to Eq. (5), it is easier for hypophosphite to

be oxidized at a lower concentration of hydrogen ion 21, which leads to a higher deposition rate as shown in curve C and D in Fig. 6.

The effects of nickel sulfate and reducer on the deposition mechanism may be classified into three types as follows according to the polarization extent and types of polarization of the partial anodic and cathodic processes 27.

Situation A: E_{dep} lies in the cathodic as well as anodic Tafel regions. Those reactions of both the anodic and the cathodic are controlled by charge-transfer. The relationship between the current density and deposition potential can be expressed in terms of the Butler-Volmer equation [40-41] based on the reactions [3] and [5], respectively.

Anodic:

$$i_a = z_a F k_{af}[H_2PO_2^-]\exp[(\beta_a n_a FE)/RT] - z_a F k_{ab}[H_2PO_3^-][H^+]\exp[(-\alpha_a n_a FE)/RT] \quad (7)$$

Cathodic:

$$i_c = z_c F k_{cf}[Ni^{2+}]\exp[(-\alpha_c n_c FE)/RT] - z_c F k_{cb}\exp[\beta_c n_c FE\}/RT] \quad (8)$$

where i, z, k, α (β), n, F, E, R, and T are the current density, number of electrons involved, rate constant, charge transfer coefficient, number of electrons involved in the rate-controlling step, Faraday's constant, electrode potential, universal gas constant, and absolute temperature respectively. The subscripts a and c represent the anodic and cathodic processes respectively, and f and b denote the forward and reverse directions of the reaction respectively. In the Tafel region, the reverse reaction is negligible. Thus, Eqs. (7) and (8) may be expressed in a simplified form as the following.

$$i_a = z_a F k_{af}[H_2PO_2^-]\exp[(\beta_a n_a FE)/RT] \quad (9)$$

$$i_c = z_c F k_{cf}[Ni^{2+}]\exp[(-\alpha_c n_c FE)/RT] \quad (10)$$

At E_{dep}, the partial current densities of the partial cathodic and anodic reaction are equal, i.e., $i_a = i_c$. Thus, one obtains

$$z_a F k_{af}[H_2PO_2^-]\exp[(\beta_a n_a FE)/RT] = z_c F k_{cf}[Ni^{2+}]\exp[(-\alpha_c n_c FE)/RT] \quad (11)$$

Assuming $n_a = n_c = 1$ and $\beta_a = \alpha_c = 0.5$, which are reasonable for a derivation of E_{dep} 28 from Eq. (11).

$$E_{dep} = \{(2.303\ RT)/F\}\log(\{k_{cf}[Ni^{2+}]\}/\{k_{af}[H_2PO_2^-]\}) \quad (12)$$

Introducing the condition of $i_a = i_c = i_{dep}$ into Eqs. (9) and (10), the deposition current density i_{dep} is given as

$$i_{dep} = 2F(k_{af}k_{cf})^{1/2} ([Ni^{2+}][H_2PO_2^-])^{1/2} \quad (13)$$

Situation B: E_{dep} lies in cathodic Tafel and anodic limiting current regions. The anodic process is diffusion-controlled, while the cathodic process is controlled by charge-transfer reaction. In this situation, E_{dep} is closer to the cathodic equilibrium potential, i_a controls the deposition rate. Thus, the anodic current density for this case is given by the Nernst's Diffusion-Layer model as 42

$$i_a = z_a F n_a D_a c_a / d_a \quad (14)$$

where D_a, c_a, and d_a are the diffusion coefficient, the bulk concentration, and the thickness of the diffusion layer, respectively, for the particular diffusing species.

At E_{dep}, $i_a = i_c = i_{dep}$, and the expression for E_{dep} could be expressed as follows using Eqs. (10) and (14).

$$E_{dep} = \{(2.303 \times 2RT)/F\} \log (\{k_{cf}\, d_a\, [Ni^{2+}]\}/\{D_a[H_2PO_2^-]\}) \quad (15)$$

and i_a in Eq. (14) stands for the i_{dep} value.

Situation C: E_{dep} lies in cathodic limiting current and anodic Tafel regions. Contrary to situation B, the cathodic process is diffusion-controlled and the anodic process is controlled by charge-transfer reaction. E_{dep} is closer to the anodic equilibrium potential, i_c controls the deposition rate. Therefore, the cathodic current density is given as follows 42.

$$i_c = z_c F n_c D_c c_c / d_c \quad (16)$$

At E_{dep}, $i_c = i_a = i_{dep}$, and the E_{dep} could be expressed as follows combining Eqs. (9) and (16).

$$E_{dep} = \{(2.303 \times 2RT)/F\} \log (\{D_c\, [Ni^{2+}]\}/\{k_{af} d_c\, [H_2PO_2^-]\}) \quad (17)$$

and i_c in Eq. (16) stands for the i_{dep} value.

The theoretical and experimental values of deposition potential and current based on the above three possible cases are listed in Table 2. Since the hydrogen evolution reaction on the cathode is neglected, the theoretical value of pH on the E_{dep} and i_{dep} should be zero in the table, which was close to the experimental value (0.02). The linear slope between log i_{dep} and log $[Ni^{2+}]$ in Fig. 3 is listed in Table 2. From a comparison the theoretically calculation (Situation A to C) with the experimental results, it indicated that the deposition rate of EN was determined by deposition potential as describe in situation A. That is to say, the EN plating probably occurred at E_{dep} in cathodic as well as anodic regions, and the deposition rate was under mixed control. It also exhibited that the deposition rate increased more effectively by increasing the concentration of the nickel ions than by increasing the concentration of the hypophosphite at lower concentration ranges from the slopes of the log i_{dep} vs. log $[Ni^{2+}]$ or log $[H_2PO_2^-]$ curves, while a reverse conclusion was gradually obtained when the concentration of metal ions extended to a much higher range.

Table 2. Expected Dependence of E_{dep} and i_{dep} on $[Ni^{2+}]$, $[H_2PO_2^-]$, and $[H^+]$

Parameter	Experimental	Situation A: Cathodic Tafel-Anodic Tafel	Situation B: Cathodic Tafel-Anodic Limiting Current	Situation C: Cathodic Limiting Current-Anodic Tafel
E_M	—	$\{(2.303RT)/F\}$ $\log(\{k_{bf}[Ni^{2+}]\}/\{k_{af}[H_2PO_2^-]\})$	$\{(2.303\times 2RT)/F\}$ $\log(\{k_{cf}[Ni^{2+}]d_a\}/\{D_a[H_2PO_2^-]\})$	$\{(2.303\times 2RT)/F\}$ $\log(\{D_c[Ni^{2+}]\}/\{k_{af}d_c[H_2PO_2^-]\})$
i_{dep}	—	$2F(k_{af}k_{cf})^{1/2}([Ni^{2+}][H_2PO_2^-])^{1/2}$	$2FD_a[H_2PO_2^-]/d_a$	$2FD_c[Ni^{2+}]/d_c$
$\delta E_{dep}/\delta\log[Ni^{2+}]$	0.10	0.07	0.14	0.14
$\delta E_{dep}/\delta\log[H_2PO_2^-]$	–0.05	–0.07	–0.14	–0.14
$\delta E_{dep}/\delta\log[H^+]$	0.02	0	0	0
$\delta\log i_{dep}/\delta\log[Ni^{2+}]$	0.62	0.50	0	1.0
$\delta\log i_{dep}/\delta\log[H_2PO_2^-]$	0.52	0.50	1.0	0
$\delta\log i_{dep}/\delta\log[H^+]$	–0.05	0	0	0

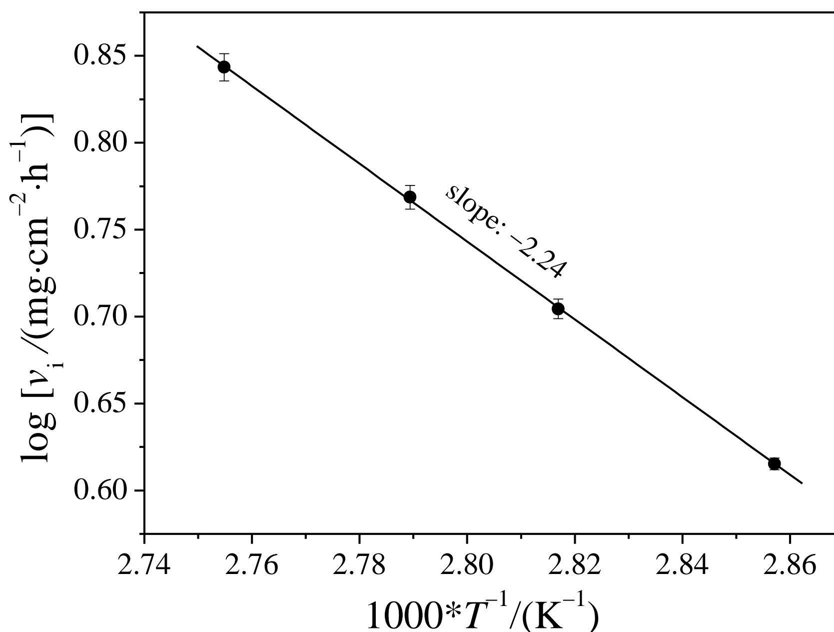

Figure 7. Logarithm of the deposition rate as a function of the reciprocal of the absolute temperature from EN in the bath composition of Table 1 ($NiSO_4\cdot 6H_2O$ 20 $g\cdot dm^{-3}$, $NaH_2PO_2\cdot H_2O$ 20 $g\cdot dm^{-3}$)

As a rule, the deposition rate of EN plating from both chemical and electrochemical reactions depended on the electrolyte temperature. The contribution from the chemical and electrochemical reactions to the process of EN plating is still in our further investigation. Fig. 7 exhibits the logarithm of the deposition rate increased linearly with the reciprocal temperature from 350 to 363 K. The apparent activation energy calculated from the slope of the Arrhenius plot was 42.89 $kJ \cdot mol^{-1}$, which was close to the values (38~45 $kJ \cdot mol^{-1}$) obtained by other investigators [14, 36] from a similar EN system.

4. CONCLUSIONS

Electrochemical behavior of EN plating in three baths was studied by polarization curves and gravimetrical techniques. The deposition rate could be calculated more precisely with the polarization curve in a complete plating bath. The value of E_{dep} increases linearly with log $[Ni^{2+}]$ and log $[H^+]$, whereas it varies inversely with respect to log $[H_2PO_2^-]$. The variation of i_{dep} on the $[Ni^{2+}]$ depends on the concentration range of nickel salt. Either a decreasing of $[H_2PO_2^-]$ or enhancement of hydrogen ion leads to a decrease i_{dep}. It is confirmed that the EN deposition is a mixed controlled electrochemical system. A monitoring technique could be developed and applied to industrial production lines.

ACKNOWLEDGMENTS
This study is jointly funded by the National Natural Science Foundation (21176061) and by Hunan Provincial Natural Science Foundation of China 12JJ2006 and the construct program of the key discipline in Hunan province.

References

1. S. Ishihara, H. Notoya, A. Okada, Z.Y. Nan, T. Goshima, *Surf. Coat. Technol*. 202 (2008) 2085.
2. B.L. Mordike, T. Ebert, *Mater. Sci. Eng*. 302 (2001) 37.
3. E.J. O'Sullivan, in: R.C. Alkire, D.M. Kolb (Eds.), Advances in Electrochemical Science and Engineering, vol., 7, Wiley-VCH, Weinheim (Germany), 2002, Ch. 5.
4. T.N. Tran, G. Yu, B.N. Hu, Z.H. Xie, R. Tang, X.Y. Zhang, *Trans. Inst. Met. Finish*. 90 (2012) 209.
5. Y.H. Xiang, W.B. Hu, X.K. Liu, C.Z. Zhao, W.J. Ding, *Trans. Inst. Met. Finish*. 79 (2001) 27.
6. M. Islam, T. Shehbaz, *Surf. Coat. Technol*. 205 (2011) 4397.
7. H. Ashassi-Sorkhabi, S.H. Rafizadeh, *Surf. Coat. Technol*. 176 (2004) 318.
8. W.L. Liu, S.H. Hsieh, H.C. Yan, W.J. Chen, *Appl. Surf. Sci*. 258 (2011) 1806.
9. Z.C. Wan, F. Jia, L. Yu, Z.B. Qi, Y. Tang, G.L. Song, *Surf. Coat. Technol*. 206 (2012) 3676.
10. W.J. Cheong, B.L. Luan, D.W. Shoesmith, *Appl. Surf. Sci.* 229 (2004) 282.
11. Y.H. Xiang, W.B. Hu, X.K. Liu, C.Z. Zhao, W.J. Ding, *Trans. Inst. Met. Finish*. 79 (2001) 30.
12. X.K. Liu, Z.L. Liu, P. Liu, Y.H. Xiang, W.B. Hu, W.J. Ding, *Trans. Nonferrous Met. Soc. China* 20 (2010) 2185.
13. J.E. Gray-Munro, B. Luan, L. Huntington, *Appl. Surf. Sci*. 254 (2008) 2871.
14. Z. Xie, G. Yu, T. Li, Z. Wu, B. Hu, *J. Coat. Technol. Res*. 9 (2012) 107.
15. W.L. Liu, S.H. Hsieh, W.J. Chen, *Thin Solid Films* 519 (2011) 4749.

16. S.S. Djokić, In: B.E. Conway, R.E. White (Eds.), Modern Aspects of Electrochemistry, vol., 35, Kluwer Academic Publishers, New York, 2002, Ch. 2.
17. J.E.A.M. VAN DEN Meerakker, *J. Appl. Electrochem*. 11 (1981) 395.
18. I. Ohno, O. Wakabayashi, S. Haruyama, *J. Electrochem. Soc*. 132 (1973) 739.
19. M. Paunovic, D. Vitkavage, *J. Electrochem. Soc*. 126 (1983) 2282.
20. I. Ohno, *Surf. Technol.* 4 (1976) 515.
21. A. Hung, I. Ohno, *J. Electrochem. Soc*. 137 (1990) 918.
22. I. Ohno, *J. Met. Finish. Soc. Jpn*. 30 (1979) 350.
23. M. Kato, K. Niikura, S. Hoshino, I. Ohno, *J. Sur. Finish. Soc. Jpn*. 42 (1991) 729.
24. S. Haruyama, A. Yoshizawa, I. Ohno, *J. Met. Finish. Soc. Jpn*. 30 (1979) 289.
25. N. Petrov, Y. Sverdlov, Y. Shacham-Diamand, *J. Electrochem. Soc*. 149 (2002) C187.
26. A. Inberg, V. Bogush, N. Croitoru, Y. Shacham-Diamand, *J. Electrochem. Soc*. 154 (2007) D1.
27. K.G. Mishra, R.K. Paramguru, *Metall. Mater. Trans*. B 30 (1999) 223.
28. K.G. Mishra, R.K. Paramguru, *J. Electrochem. Soc*. 143(1996) 510.
29. J. Li, P.A. Kohl, *J. Electrochem. Soc*. 149 (2002) C631.
30. P. Bindra, J. Roldan, *J. Appl. Electrochem*. 17 (1987) 1254.
31. B.D. Barker, D. Taberner, *Surf. Technol*. 12 (1981) 103.
32. I. Ohno, S. Haruyama, *Surf. Technol*. 13 (1981) 1.
33. L.M. Abrantes, J.P. Correia, *J. Electrochem. Soc*. 141 (1994) 2356.
34. Z. Xie, G. Yu, B. Hu, X. Lei, T. Li, J. Zhang, *Appl. Surf. Sci*. 257 (2011) 5025.
35. F. Yang, B. Yang, B. Lu, L. Huang, S. Xu, S. Zhou, *Acta Phys.- Chim. Sinica* 22 (2006) 1317.
36. M.Y. Abyaneh, A. Sterritt, T.J. Mason, *J. Electrochem. Soc*. 154 (2007) D467.
37. A. Malecki, A. Micek-Ilnicka, *Surf. Coat. Technol*. 123 (2000) 72.
38. L. Gui, in: M. Wu (Ed.), Handbook of Materials Testing for Mechanical Engineering, vol: Corrosion and Friction, Liaoning Science and Technology Press, Liaoning (China), 2002, Ch. 1.
39. S.M. El-Raghy, A.A. Abo-Salama, *J. Electrochem. Soc*. 126 (1979) 171.
40. L. Gorker, V. Dimitrov, *Prog. React. Kinet. Mech*. 34 (2009) 127.
41. Y.D. Gamburg, G. Zangari, Theory and Practice of Metal Electrodeposition, Springer, New York (2011).
42. N. Kanani, Electroplating: Basic Principles, Processes and Practice, Elsevier, Oxford UK (2004).

© 2013 by ESG (www.electrochemsci.org)